Journal of Power Sources 195 (2010) 7181–7186

Contents lists available at ScienceDirect

Journal of Power Sources

journal homepage: www.elsevier.com/locate/jpowsour

Applicability of extra low interstitials ferritic stainless steels for bipolar plates of proton exchange membrane fuel cells

Masanobu Kumagai [a], Seung-Taek Myung [b,*], Takuma Ichikawa [b], Hitoshi Yashiro [b,*]

[a] Taiyo Stainless Spring Co., Ltd., 2-8-6 Shakujiicho, Nerimaku, Tokyo 177-0041, Japan
[b] Department of Chemical Engineering, Iwate University, 4-3-5 Ueda, Morioka, Iwate 020-8551, Japan

ARTICLE INFO

Article history:
Received 9 April 2010
Accepted 11 May 2010
Available online 20 May 2010

Keywords:
Ferritic stainless steel
Corrosion
Bipolar plates
Fuel cell
XPS

ABSTRACT

Ferritic stainless steels can be attractive bipolar plate materials of proton exchange membrane fuel cells (PEMFC), provided that the stainless steels show sufficient corrosion resistance, for instance, by eliminating interstitial elements such as carbon and nitrogen. In the present study, thus, ferritic stainless steels (19Cr2Mo and 22Cr2Mo) with extra low interstitials (ELI) are evaluated to determine the required level of chromium content to apply them for PEMFC bipolar plates. In a simulated PEMFC environment (0.05 M SO_4^{2-} (pH 3.3) + 2 ppm F^- solution at 353 K), the 22Cr2Mo stainless steel showed lower current density during the polarization in comparison with the 19Cr2Mo one. The polarization behavior of the 22Cr2Mo stainless steel resembles that of the type 316 one (17Cr12Ni2Mo). Similar values of interfacial contact resistance (ICR) are observed for both ferritic stainless steels. The 22Cr2Mo stainless steel bipolar plate is found to be stable throughout the cell operation, while the 19Cr2Mo stainless steel corroded within 1000 h. After the cell operation, the 22Cr2Mo stainless steel retains the chromium enriched passive film, while the chromium enriched surface film is not found for the 19Cr2Mo one, showing iron oxide/hydroxide based film. X-ray fluorescence (XRF) analysis of the membrane electrode assemblies (MEAs) after the cell operation indicates that the 22Cr2Mo stainless steel was less contaminated with iron species. The above results suggest that the 22Cr2Mo stainless steel can be applicable to bipolar plates for PEMFC, especially 22 mass% of chromium content in ferritic stainless steel with ELI system is, at least, demanded to ensure stable cell performance.

© 2010 Elsevier B.V. All rights reserved.

1. Introduction

Proton exchange membrane fuel cells (PEMFC) principally are composed of membrane electrode assembly (MEA) and bipolar plates. Bipolar plates are estimated to occupy 45% of PEMFCs stack cost [1,2]. Practical bipolar plates need to be approved in terms of cost, corrosion resistance, interfacial contact resistance (ICR) against gas diffusion layer (GDL), mechanical strength, and impermeability by reactant gases in PEMFC environments. Since stainless steel generally meets those requirements, a great deal of attention has been paid to it.

There are many works [3–16] that austenitic stainless steels [3–13] and Ni-based alloy [14–16] bipolar plates have preferable corrosion resistance in the real PEMFC environments. For example, types 316L [3,6,7], 310S [4,8,9–13] and 904L [5] stainless steels have been proposed as promising materials by Davies et al. [4,5]: the cell performance improved with increasing chromium and nickel contents in the stainless steel. In general, addition of chromium and nickel is common to improve corrosion resistance of stainless steel. However, higher contents of chromium and nickel in the stainless steel lead to high cost bipolar plate. Less attention has been directed to ferritic stainless steels, probably because they generally exhibit inferior corrosion resistivity and machinability to austenitic stainless steels. Even though nickel ingredient is not contained in ferritic stainless steels, they are immune to stress corrosion clacking (SCC) even above 353 K [17]. Also, absence of nickel ingredient would positively affect cell performance because adherence of nickel ions deteriorates MEA performance [6], resulting degradation of cell performance. Previous study by Wang and Turner [18] suggested that ferritic series of stainless steels such as AISI 434, 436, 441 and 444 did not show sufficient corrosion resistance under their simulated PEMFC environment. Increasing chromium content to 28 wt.% with a small amount of nickel addition (AISI 446) gave rise to formation of stable passive films providing high corrosion resistance.

Recent development of ferritic stainless steels with extra low interstitials (ELI) has enabled them to be improved in corrosion resistance as much as austenitic stainless steels at the similar level of chromium content [17]. It can be claimed that ferritic stainless steels intrinsically have higher ICR against GDL as compared

* Corresponding authors. Tel.: +81 19 621 6345; fax: +81 19 621 6345.
E-mail addresses: smyung@iwate-u.ac.jp (S.-T. Myung), yashiro@iwate-u.ac.jp (H. Yashiro).

0378-7753/$ – see front matter © 2010 Elsevier B.V. All rights reserved.
doi:10.1016/j.jpowsour.2010.05.025

Table 1
Chemical compositions of specimens.

	C	Si	Mn	Cr	Ni	Mo	N	Fe
22Cr2Mo	0.008	0.40	0.20	21.75	–	2.06	0.007	Bal.
19Cr2Mo	0.009	0.63	0.20	18.73	–	2.12	0.013	Bal.
17Cr12Ni2Mo	0.010	0.51	0.51	17.10	11.96	1.99	0.046	Bal.

to austenitic stainless steels [18]. To reduce the ICR at the similar level to graphite, however, surface modification is necessary for all stainless steels, except some kinds of special stainless steels containing boron-based [19,20] and carbon-based metal [21,22]. Since we have already developed an effective method to improve ICR between GDL and stainless steels [9,12], the problem of ICR for a bare ferritic stainless steel with GDL is not a critical issue. We, thus, focused on corrosion resistivity of ferritic stainless steels to find the optimum level of chromium content that meets the requirement under the PEMFC environment.

In the present study, ferritic stainless steels with ELI of which the chromium content is addressed from 19 to 22 mass% are investigated. Here, we report electrochemical tests, fuel cell performance and applicability of the ferritic stainless steel with ELI for bipolar plates as substrate material for PEMFCs.

2. Experimental

Two types of commercially available ferritic stainless steels with ELI, namely type 444 (19Cr2Mo) and type 445J2 (22Cr2Mo), with different contents of chromium were compared (see Table 1). Type 316 (17Cr12Ni2Mo) stainless steel was employed to understand the effect of nickel for comparison, although the chromium content was slightly lower than the 19Cr2Mo stainless steel. Those stainless steels were provided by Nippon Metal Industry Co. Ltd. The chemical compositions of the above stainless steels are described in Table 1. The stainless steel plates were machined into a square (20 mm × 20 mm × 2 mm) and mounted into epoxy resin for polarization tests. Surfaces of the specimens were finished using diamond paste polisher of 6 μm and cleaned ultrasonically in hexane for 15 min.

Polarization tests were carried out in PTFE lined cells which were filled with 200 cm^3 of 0.05 M SO_4^{2-} (pH 3.3) + 2 ppm F^- solution saturated with either Ar (dynamic mode: −500 to +1500 mV with a sweep rate of 60 mV min^{-1}) or air (transient mode: at +600 mV for 8 h) to simulate the PEMFC cathode environments [23]. A reference electrode (SCE) was placed out of the water bath which kept the temperature of the cell to 353 K. Prior to the anodic polarization test, specimens were scanned first to −500 mV (SCE) to remove air-formed oxide films.

The stainless steel plates were also machined into bipolar plates (80 mm × 80 mm × 6 mm) with a serpentine flow field according to the NEDO report by JARI [24]. The surfaces of the bipolar plates were equally finished using diamond paste polisher of 6 μm and cleaned ultrasonically in hexane for 15 min. Active area of each electrode area was 50 mm × 50 mm. A single cell was assembled from the stainless steel bipolar plates and a commercially available MEA employing carbon cloth GDL with a compressive force of 150 N cm^{-2} controlled by a torque wrench. The single cell was operated at 348 K under ambient pressure (FC5105M, CHINO). The reactant gases were fully humidified at 343 K. The utilization was 70% for the fuel gas (H_2) and 40% for air. The applied current density was 0.5 A cm^{-2}.

After the polarization tests and single cell operations, the surfaces of the stainless steel bipolar plates were analyzed by X-ray photoelectron spectroscopy (XPS, ULVAC-PHI 5600) with a monochromatic Al Kα source. The take-off angle of the emitted photoelectrons was adjusted to 45° with respect to the surface.

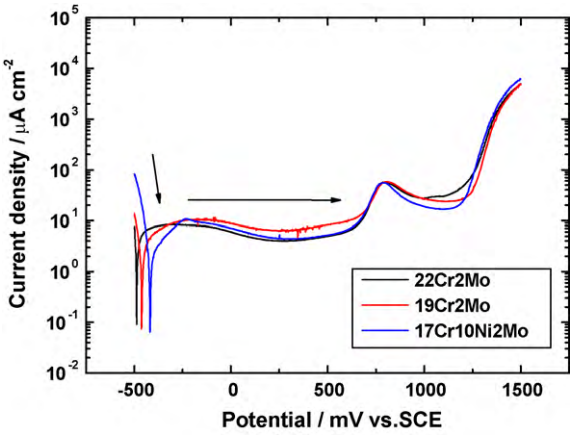

Fig. 1. Anode polarization curves for the 17Cr12Ni2Mo, 19Cr2Mo and 22Cr2Mo stainless steel in deaerated 0.05 M SO_4^{2-} (pH 3.3) + 2 ppm F^- solution at 353 K.

Binding energies of XPS peaks of standards were referred from literature [25]. X-ray fluorescence (XRF, Philips Magix PRO-S) was employed to quantify the MEA contamination after the cell operation for 1000 h.

3. Results and discussion

Fig. 1 shows anodic polarization curves of the three kinds of stainless steel specimens in 0.05 M SO_4^{2-} (pH 3.3) + 2 ppm F^- solutions at 353 K. Apparent corrosion potentials lie around −480 mV (SCE) for the 19Cr2Mo and the 22Cr2Mo stainless steels. On the other hand, the corrosion potential for the 17Cr12Ni2Mo stainless steel appears at about −350 mV (SCE). A little higher corrosion potential is recognized for the 17Cr12Ni2Mo stainless steel, probably because of the more activated hydrogen evolution reaction for the nickel containing austenitic stainless steel. At the potential range from −200 mV (SCE) to +700 mV (SCE), the current densities for the three stainless steels are almost constant owing to the formation of stable passive films. A large peak is observed in the potential range from +700 mV (SCE) to +1200 mV (SCE). The change into transapassivation is attributed to the formation of hexavalent chromate ion. Nickel seems to play no role on the transpassivation reaction.

Since type 304 stainless steel bipolar plate was corroded more seriously on the cathode side according to our previous studies [8,10], polarization tests were carried out in the synthesized cathodic environment. Fig. 2 shows current density versus time

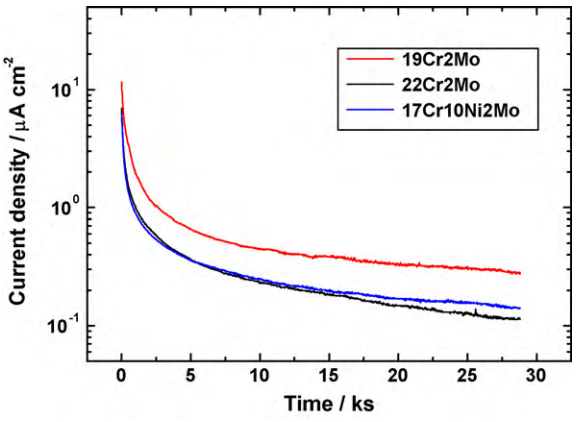

Fig. 2. Change of time variation for the 17Cr12Ni2Mo, 19Cr2Mo and 22Cr2Mo stainless steel in deaerated 0.05 M SO_4^{2-} (pH 3.3) + 2 ppm F^- solution at 353 K.

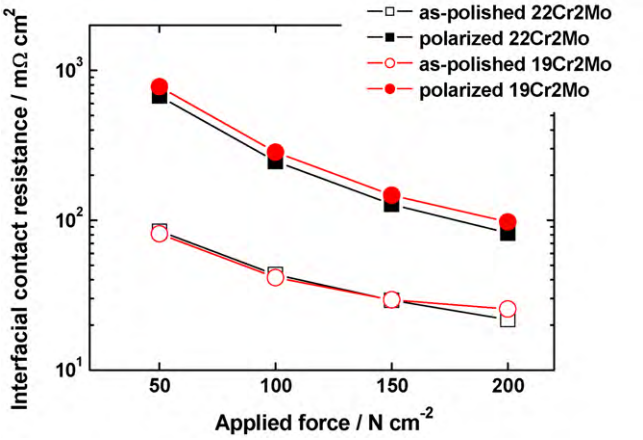

Fig. 3. Contact resistance between the 19Cr2Mo and 22Cr2Mo stainless steel and carbon cloth after polarization at +600 mV (SCE) for 8 h in 0.05 M SO_4^{2-} (pH 3.3) + 2 ppm F^- solution at 353 K.

curves for the three stainless steels polarized at +600 mV (SCE) in 0.05 M SO_4^{2-} (pH 3.3) + 2 ppm F^- solution at 353 K. The transient current density decays very fast for every stainless steel in early 1000 s due to formation of passive films. As soon as the surface is covered with the passive film, the current density becomes lower to maintain the passivation. As shown in Fig. 2, the current densities of the 22Cr2Mo and 17Cr12Ni2Mo (type 316) stainless steels are apparently lower than that of the 19Cr2Mo stainless steel during polarization for 8 h. This indicates that the corrosion resistance of the 22Cr2Mo stainless steel is quite close to that of the type 316 one.

Fig. 3 shows the interfacial contact resistance (ICR) between the carbon cloth GDL and ferritic stainless steels in the as-polished and the post-polarized states. The measurement method referred to literature [4]. The two stainless steels show similar ICR values in the as-polished state. Polarization of the stainless steels for 8 h at +600 mV (SCE) raises the ICR values. This is probably due to the higher content of chromium in the surface oxide layer, as will be mentioned later.

XPS analysis was performed to investigate the surface state of the stainless steels before and after the polarization. As can be seen in Fig. 4(a), all the as-polished and the polarized stainless steels show a peak at around 707 eV, which corresponds to iron metal. A composite peak for iron oxide/hydroxide is observed at around 711 eV for the as-polished stainless steels. However, this peak becomes weaker after the polarization. In Fig. 4(b), a small peak is seen for every specimen at around 574 eV, which is ascribed to chromium metal. The peak for chromium oxide/hydroxide as observed at around 577 eV becomes stronger. This indicates that the iron oxide/hydroxide on the passive films are mostly dissolved into the synthetic solution of pH 3.3, resulting in relative enrichment of chromium oxide/hydroxide on the outer surface of both stainless steels.

Fig. 5 shows cationic ratio of chromium versus iron in the films formed on the 19Cr2Mo and the 22Cr2Mo stainless steels before and after the polarization in 0.05 M SO_4^{2-} (pH 3.3) + 2 ppm F^- solution at 353 K. For the as-polished stainless steels, iron oxide/hydroxide constitutes the majority of the passive film. On the other hands, the stainless steel surface is covered mainly with chromium oxide/hydroxide in the polarized state. The cationic ratio of the chromium species in the passive films reaches approximately 70% for the 19Cr2Mo and 72% for the 22Cr2Mo stainless steels. The results are quite similar to those for austenitic stainless steels in our prior study [10].

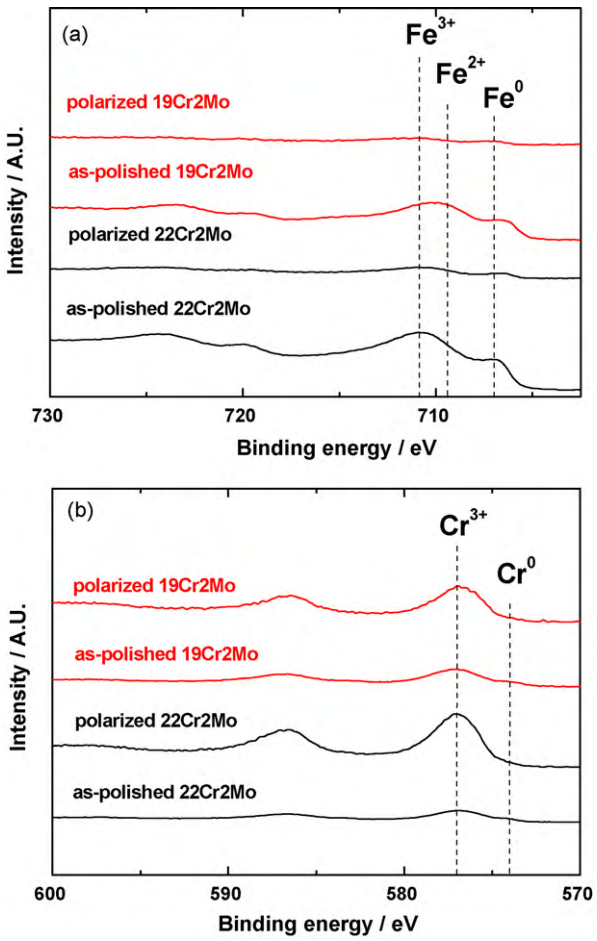

Fig. 4. XPS spectra of (a) Fe2p and (b) Cr2p for the 19Cr2Mo and 22Cr2Mo stainless steel after 8 h polarization at +600 mV (SCE) in 0.05 M SO_4^{2-} (pH 3.3) + 2 ppm F^- solution at 353 K.

We mentioned that the higher ICR value of the 22Cr2Mo stainless steel is ascribed to the higher content of chromium in the passive film. Indeed, electronic conductivity of chromium oxide is lower than that of iron oxide. For this reason, the higher ICR value for the 22Cr2Mo stainless steel that contains more amount of chromium oxide in the passive film is explained.

Single cells were fabricated using those bipolar plates to evaluate the stainless steel bipolar plates in the real PEMFC environment.

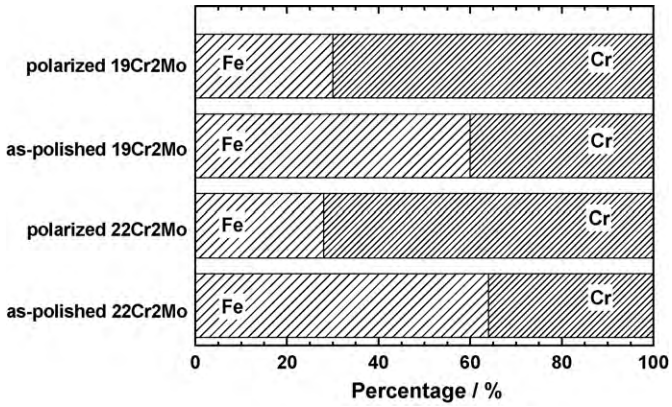

Fig. 5. Chromium oxide/iron oxides cationic ratio based on XPS analysis for the 19Cr2Mo and 22Cr2Mo stainless steel polarized at +600 mV for 8 h in 0.05 M SO_4^{2-} (pH 3.3) + 2 ppm F^- solution at 353 K.

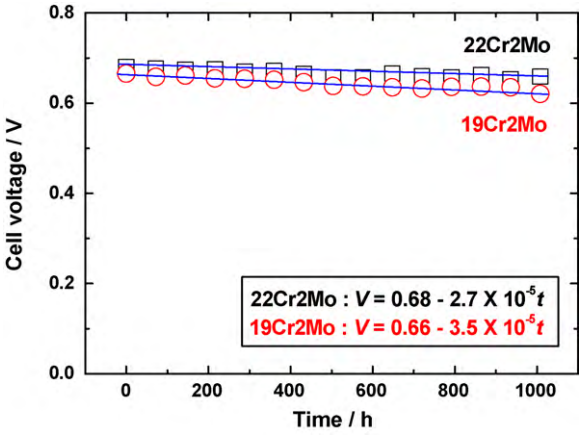

Fig. 6. Change of cell voltage for the 19Cr2Mo and 22Cr2Mo stainless steel bipolar plate employing single cell at a constant current of 0.5 A cm^{-2} (348 K).

The assembled cells are operated for 1000 h at 0.5 A cm^{-2}. Fig. 6 shows the time variation of the cell voltage during the 1000 h operation. A cloth type of GDL is used for MEA. For the 19Cr2Mo stainless steel employing cell, the initial cell voltage is approximately 0.66 V and the voltage decay is 35 mV in 1000 h. In the case of the 22Cr2Mo stainless steel bipolar plates employing cell, the initial cell voltage is slightly higher, approximately 0.68 V. It shows higher voltage retention during operation and the voltage decay was approximately 27 mV upon 1000 h operation. Apparently, the 22Cr2Mo stainless steel bipolar plates employing cell exhibits improved single cell performance.

The operated cells were carefully disassembled and the bipolar plates were observed by the metallurgical microscope in Fig. 7. Both stainless steel bipolar plates on the anode side were not corroded (Fig. 7(a) and (c)). On the other hand, the 19Cr2Mo stainless steel bipolar plate (Fig. 7(b)) on the cathode side was corroded despite that the 22Cr2Mo (Fig. 7(d)) did not present corrosion. The increment of chromium content to 22% seems to effectively delay the corrosion. Thus, it is speculated that the higher operation voltage could be maintained throughout the operation for the 22Cr2Mo stainless steel bipolar plate employing cell in Fig. 6. This implies that higher content of chromium in the metal bulk is preferred to improve the corrosion resistance even in ferritic stainless steel system, as evidenced in Figs. 6 and 7. From the view point, we believe that 22 wt.% of chromium is at least necessary to guaranty the cell performance, although nickel is not incorporated in the metal balk.

The surfaces of the bipolar plate on the cathode side were also examined by XPS in Fig. 8. For the 19Cr2Mo stainless steel bipolar plates, the iron metal at around 707 eV is barely observed in Fig. 8a, whereas the metal peak is clearly seen for the 22Cr2Mo stainless steel. On the other hand, the iron oxide/hydroxide peak at around 711 eV is strongly observed for the 19Cr2Mo stainless steel bipolar plate, compared with the 22Cr2Mo stainless steel. As shown in Fig. 7(b), those corrosion products covering the most outer surface would have resulted in the strong reflection of the iron oxide/hydroxide peak. Meanwhile, absence of the corrosion product for the 22Cr2Mo stainless steel means that the XPS spectrum reflects the passive film of the stainless steel. It seems that the oxide layer is not so thick since the iron metallic component is clearly visible in Fig. 8(a). For Cr2p spectra, the chromium metal at around 574 eV and chromium oxide/hydroxide at 577 eV for the 22Cr2Mo stainless steel bipolar plate is clearly observed. The rela-

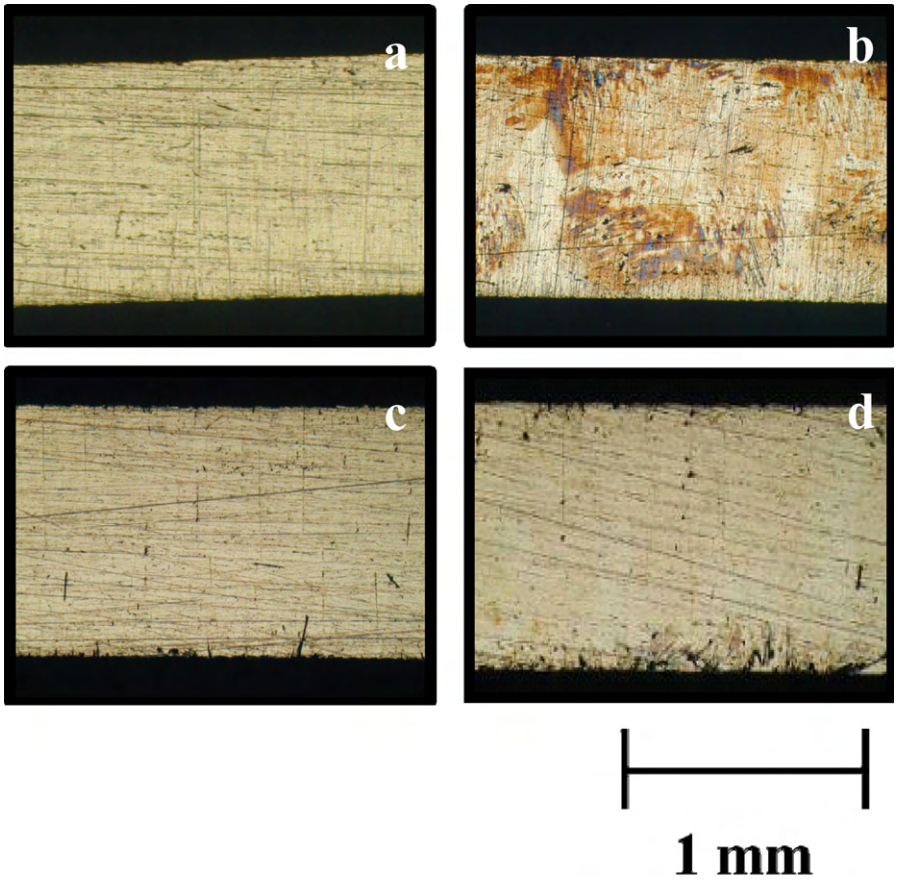

Fig. 7. Metallurgical microscope images of the rib surfaces after 1000 h; (a) anode side of the 19Cr2Mo, (b) cathode side of the 19Cr2Mo, (c) anode side of the 22Cr2Mo and (d) cathode side of the 22Cr2Mo. The scale bar indicates 1.0 mm.

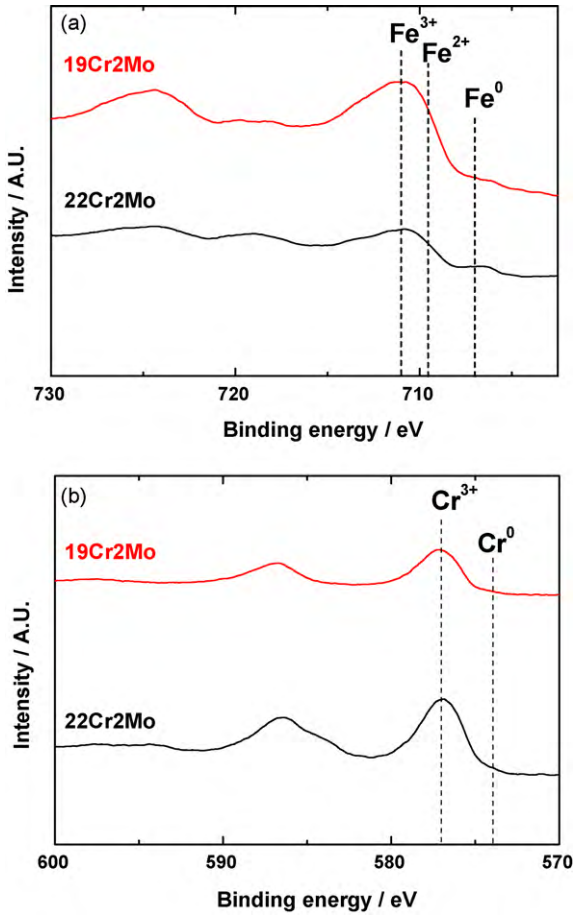

Fig. 8. XPS spectra of (a) Fe2p and (b) Cr2p for the 19Cr2Mo and 22Cr2Mo stainless steel bipolar plates on the cathode side after 1000 h cell operation.

tive intensities of chromium oxide for the 19Cr2Mo stainless steel appear relatively weak. The cationic ratio of chromium versus iron within the oxide layer based on the XPS analysis is 22:78 for the 19Cr2Mo and 59:41 for the 22Cr2Mo stainless steel, respectively. The XPS results indicate that the 22Cr2Mo bipolar plates keep passivity over the course of cell operation, while the 19Cr2Mo suffer from general corrosion.

From the XPS investigation, we found that the corrosion product which covered the 19Cr2Mo stainless steel bipolar plate consists of iron oxide/hydroxide. The formed iron oxide/hydroxide would be led by the consecutive process: (I) release of Fe^{2+} ion from the stainless steel that constitutes the passive film and (II) oxidation of Fe^{2+} ion and deposition on the passive film. During the process some of Fe^{2+} ion can be incorporated into the MEA. In this case, the presence of Fe^{2+} ion would disturb the proton exchange and it may be remained as inactivated part, bringing about cell voltage decay. Thus, MEAs for the 19Cr2Mo and 22Cr2Mo after 1000 h operation are measured by XRF. To avoid the contamination of iron from a cutter, WC-coated cutter is used. The MEA combined with the 19Cr2Mo stainless steel bipolar plate exhibits the higher contamination with iron, as compared with the case of the 22Cr2Mo stainless steel. The concentration of chromium in the MEA is under the detection level for the both cases. This result agrees with the optical microscopic images shown in Fig. 7. Namely, as the bipolar plate corrodes more, more amount of iron ingredient is found in MEA (Fig. 9).

Therefore, it is concluded that retaining the higher cell operation voltage can be achieved using bipolar plates of ferritic stainless steel with ELI containing higher than 22 wt.% chromium content.

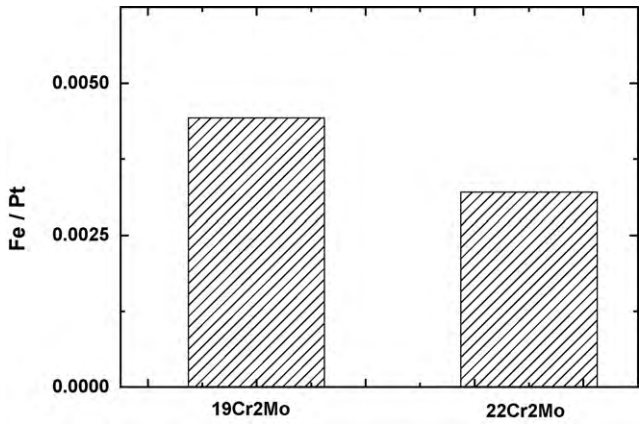

Fig. 9. XRF results of MEA for the 19Cr2Mo and 22Cr2Mo stainless steel bipolar plates employing single cell after 1000 h operation.

4. Conclusions

Ferritic stainless steels with enhanced corrosion resistance produced by elimination of interstitial elements (19Cr2Mo and 22Cr2Mo) were evaluated as a bipolar plate of PEMFCs.

In the simulated PEMFC environment, the polarized ferritic stainless steels at +600 mV (SCE) showed smaller anodic current density, compared with austenitic type 17Cr12Ni2Mo stainless steel. The polarized steels in the simulated cathode condition were covered mainly with chromium oxide/hydroxide, as confirmed by XPS. In the real PEMFC environment, the cell voltage was kept better for the 22Cr2Mo stainless steel bipolar plates employing cell, compared with 19Cr2Mo. There formed chromium enriched passive film on the 22Cr2Mo stainless steel bipolar plate, while 19Cr2Mo stainless steel bipolar plates are covered with iron oxide/hydroxide after 1000 h cell operation. The MEA was more contaminated with iron species for the 19Cr2Mo stainless steel bipolar plates employing cell.

We would suggest that more than 22 wt.% of chromium content in the ferritic stainless steel with ELI is demanded for the PEMFCs bipolar plate.

Acknowledgements

The authors thank Ms. Miwa Watanabe, Iwate University, and Mr. Takahito Takagawa, Iwate Industrial Research Center (XRF), for their helpful assistance in the experimental work and Nippon Metal Industry Co. Ltd. for the supply of stainless steel. This research was partially supported by the Ministry of Education, Science, Sports and Culture, Grant-in-Aid for Scientific Research (c), 20560665, 2008–2010.

References

[1] B.C.H. Steele, A. Heinzel, Nature (London) 414 (2001) 345.
[2] H. Tsuchiya, O. Kobayashi, Int. J. Hydrogen Energy 29 (2004) 985.
[3] P.L. Hentall, J. Barry Lakeman, G.O. Mepsted, P.L. Adcock, J.M. Moore, J. Power Sources 80 (1999) 235.
[4] D.P. Davies, P.L. Adocock, M. Turpin, S.J. Rowen, J. Appl. Electrochem. 30 (2000) 101.
[5] D.P. Davies, P.L. Adocock, M. Turpin, S.J. Rowen, J. Power Sources 86 (2000) 237.
[6] J. Wind, R. Spah, W. Kaiser, G. Bohm, J. Power Sources 105 (2002) 256.
[7] E.A. Cho, U.-S. Jeon, S.-A. Hong, I.-H. Oh, S.-G. Kang, J. Power Sources 142 (2005) 177.
[8] H. Yashiro, R. Asaishi, S. Kuwata, M. Kumagai, A. Yao, Trans. Mater. Res. Soc. Jpn. 32 (2007) 963.
[9] S.-T. Myung, M. Kumagai, R. Asaishi, Y.-K. Sun, H. Yashiro, Electrochem. Commun. 10 (2008) 480.
[10] M. Kumagai, S.-T. Myung, S. Kuwata, R. Asaishi, H. Yashiro, Electrochim. Acta 53 (2008) 4205.

[11] M. Kumagai, S.-T. Myung, R. Asaishi, Y. Katada, H. Yashiro, J. Power Sources 185 (2008) 815.
[12] M. Kumagai, S.-T. Myung, R. Asaishi, Y.-K. Sun, H. Yashiro, Electrochim. Acta 54 (2008) 574.
[13] M. Kumagai, S.-T. Myung, S. Kuwata, R. Asaishi, Y. Katada, H. Yashiro, Electrochim. Acta 54 (2009) 1127.
[14] M.P. Brady, K. Weisbrod, I. Paulauskas, R.A. Buchanan, K.L. More, H. Wang, M. Wilson, F. Garzon, L.R. Walker, Scripta Mater. 58 (2004) 1017.
[15] M.P. Brady, B. Yang, H. Wang, J.A. Turner, K.L. More, M. Wilson, F. Garzon, JOM J. Met. Miner. Mater. Soc. 58 (2006) 50.
[16] M.P. Brady, H. Wang, B. Yang, J.A. Turner, M. Bordignon, R. Molins, M. Abd Elhamid, L. Lipp, L.R. Walker, Int. J. Hydrogen Energy 32 (2007) 3778.
[17] Y. Hosoi, Zairyo-to-Kankyo 56 (2007) 439.
[18] H. Wang, J. Turner, J. Power Sources 128 (2004) 193.
[19] Japanese Patent P-2000-328200A (2000).
[20] Japanese Patent P-2000-328205A (2000).
[21] Japanese Patent P-2000-303151A (2000).
[22] Japanese Patent P-2000-309854A (2000).
[23] R.L. Borup, N.E. Vanderborgh, Mater. Res. Soc. Symp. Proc. 393 (1995) 151.
[24] Japan Automobile Research Institute, NEDO Report, 2001, p. 21.
[25] C.D. Wagner, W.M. Riggs, L.E. Davis, J.F. Moulder, Handbook of X-Ray Photoelectron Spectroscopy, Perkin Elmer Corp., Physics and Electronics Division, Eden Prairie, MN, 1979.